Leino, Mikko K.; Bergman, Jan; Ala-Laurinaho, Juha; Viikari, Ville

Beam Optimization for 28 GHz Phased Array Utilizing Measurement Data

Published in:
14th European Conference on Antennas and Propagation, EuCAP 2020

DOI:
10.23919/EuCAP48036.2020.9135596

Published: 01/03/2020

Document Version
Peer-reviewed accepted author manuscript, also known as Final accepted manuscript or Post-print

Beam Optimization for 28 GHz Phased Array Utilizing Measurement Data

Mikko K. Leino, Jan Bergman, Juha Ala-Laurinaho, and Ville Viikari
Department of Electronics and Nanoengineering, Aalto University School of Electrical Engineering, Espoo, Finland
mikko.k.leino@aalto.fi

***Abstract*—This paper presents beam optimization methods for a phased array operating at 28 GHz. The phase of each antenna element is controlled with an element-specific 5-bit phase shifter. The amplitude of each element varies with the chosen phase shift state due to the antenna design. Each individual element is measured and based on the measurement data, the beam optimization for the maximum gain is done. The optimization increases the measured gain compared to the nominal case by 1.3 dB at broadside. Furthermore, the element amplitude variation allows optimization for the lower side lobes to be done by finding the correctly weighted amplitudes. Taylor distribution is used for this optimization and the side-lobe level decreases 2.4 dB for the broadside beam.**

***Index Terms*—Beam steering, Phased arrays, Phase shifters.**

I. Introduction

Future 5G antennas are required to operate at millimeter waves with low-losses and high efficiency. This necessitates that the radiated power is directed to the wanted direction to maximize the link budget. The beam must be steerable to focus the energy to the receiver, and preferably also reconfigurable so that side lobe level can be controlled or beam width adjusted for decreased interference. Phased arrays are good solution for these requirements, as they can be easily designed to support flexible beamforming.

The shaping of the phased array beam is usually realized by adjusting the element phases with electronically controlled phase shifters. This allows the beam steering in two dimensions for planar arrays. Other way to affect the antenna beam includes the control of the element amplitudes [1]. For example, with weighted excitation, the side-lobe level can be decreased compared to the uniform excitation. However, the trade-off is lower gain.

The phased arrays normally require a calibration or optimization as the array elements have error in amplitude and phase usually caused by the phase shifters, but also by the feeding network, and due to possible impedance mismatch between the phase shifters, feed network, and antenna elements. Beam pointing errors have been studied [2] and quite often the phase correction is applied to negate this and increase the gain [3], [4]. In addition, the amplitude errors due to the phase shifter losses should not be neglected [5]. Experimental studies on how to maximize the transmitted power, i.e. the gain, has been presented before [6] and the results are usually quite application specific.

We present two beam-optimization methods for a phased array operating at 28 GHz. The main method maximizes the antenna gain while the other is for reducing the side lobes. Amplitudes and phases of each element have been measured individually for all phase shifter states. Both optimization methods utilize this data to achieve the required goals.

The measurement data are achieved for each element when the others are turned off to ensure that the measurement data are usable for the optimization. One way to obtain amplitude and phase data that also takes into account the mutual coupling is to observe holography data for all the elements like in [7]. However, this should be done for all the possible phase shifter state configurations which are too time-consuming and laborious to be separately measured.

II. Phased Array

Waveguide-based phased array operating at 28 GHz and suitable for 5G backhauling has been presented in [8]. This antenna provides low-losses compared to the traditional planar realizations due to the waveguide-based feeding network and horn antennas. The antenna has 16 elements whose phases are controlled with individual 5-bit phase shifters. These digital phase shifters are mounted on the PCB which is installed between the power division network and the horn antenna array. Thus, transitions between the waveguides and the microstriplines on the PCB are also present in the design. More in-depth description of the antenna can be found in [8].

The antenna element numbering and the steering directions are presented in Fig. 1. The antenna is fed from one port and the feeding network is designed to distribute the power evenly so that the elements would be uniformly excited. However, the output phase of the feeding network for each element is not the same. This element-specific initial phase has to be taken into account when steering the beam.

The antenna beam is steered by applying progressive phase shift between the elements according to the required steering angle. The phase shifters are assumed to operate rather ideally. The 5-bit digital phase shifter offers 32 different phase states nominally offset by 11.25°. The first state is chosen as the reference state (State 1) i.e. its phase is 0° which determines the phase of the other states according to the nominal offset.

However, some error sources are neglected in this ideal beam forming. The aforementioned initial phases of each element are taken from the simulations. In reality, the actual values may have drifted a bit from the simulated ones. Furthermore, the phase and amplitude errors of the phase shifters are not considered. To correct these issues, the element phases

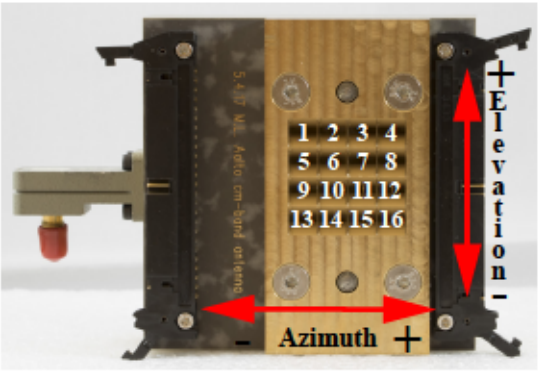

Fig. 1. Antenna prototype with element numbering and the beam steering directions.

have been adjusted towards the broadside in [8]. This adjustment provides 0.6 dB increase in gain, but is rather arduous to do for each steering angle. In addition, the phase state (State 1) in the reference element (Element 1) is kept the same in this calibration. This means that other subsets of element phase shifter states that would provide the same progressive phase shift between the elements are not considered. This is a problem because the element amplitude varies with the chosen state.

III. Antenna Element Measurements

The signal path after the power division network is the following: First there is a transition from the waveguide to the microstripline on the PCB. Wire bonded phase shifter on the PCB changes the signal phase. Microstrip to waveguide transition is last used to guide the signal to a horn antenna. The transmission coefficient of the phase shifter added in between the transitions is simulated to analyze the element amplitude variation. The simulations are done with every phase state and the average transmission coefficient is calculated. The result is shown in Fig. 2 and the variation depending on the chosen state is also highlighted.

Depending on the chosen phase shifter state, the transmission coefficient in the single element path can vary significantly. Peak-to-peak difference is 1.7 dB at 28 GHz according to the simulations. Small variation might be explained by the amplitude deviation between the different phase states, but this large discrepancies are likely due to the matching. The matching between the phase shifter and the microstrip line is not that good causing reflections. Furthermore, there are matching problems in the transitions between waveguides and the PCB. The two transitions are rather sensitive to the phase deviation and the matching between waveguides and the PCB is deteriorated due to that.

However, the actual amplitude variations are even larger and can change from element to element, because the transmission coefficient simulations do not take into account the feeding network as it affects the matching substantially. To find out the actual amplitude fluctuation, the phase and amplitude of each antenna element are measured with different phase states. Measurements are done by placing a probe right in front of the measured element while the other elements are turned off. This is done to ensure the measured results are precise enough to be used in the optimization. In these measurements the phase and amplitude of each phase state are recorded for the measured element at different frequencies.

The normalized average amplitude for the center element 6 is shown in Fig. 3 and the variation depending on the chosen phase shifter state is again highlighted. The measured amplitudes are normalized to the attained maximum value over all the elements. At 28 GHz the amplitude deviation is significant, 6.2 dB from peak-to-peak. Similar results are also achieved with other elements.

IV. Beam Optimization

A polar plot for a single element visualizing the measured phase and amplitude response for every phase state is presented in Fig. 4. Again the element in question is the center element 6 and the observation frequency is 28 GHz. The amplitudes in this presentation are normalized to the maximum amplitude of the plot. The phase of the first state is set to 0° and the phase of the rest of the states are relative to this value.

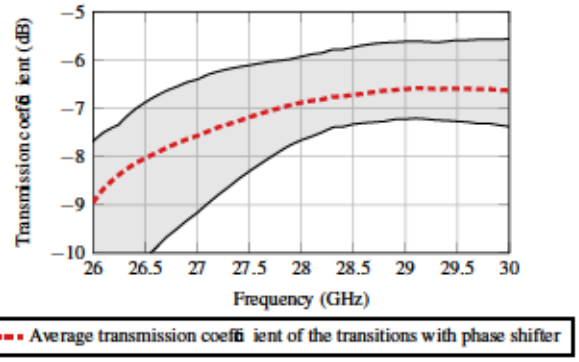

Fig. 2. Simulated average transmission coefficient including both transitions and phase shifter. The variation depending on the chosen phase shifter state is highlighted. Note that the specified phase shifter operation range is 28–32 GHz.

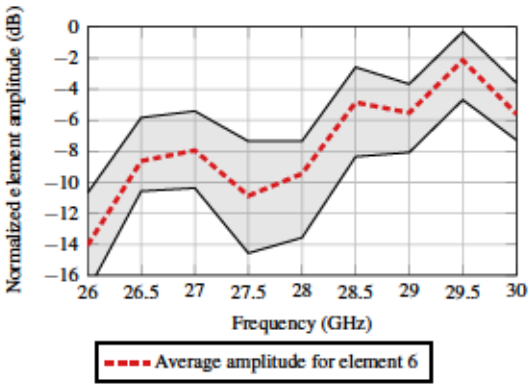

Fig. 3. Measured average amplitude for the element 6. Amplitudes are normalized to the measured maximum value over all the elements and over the frequency range 26–30 GHz. The variation depending on the chosen phase shifter state is highlighted.

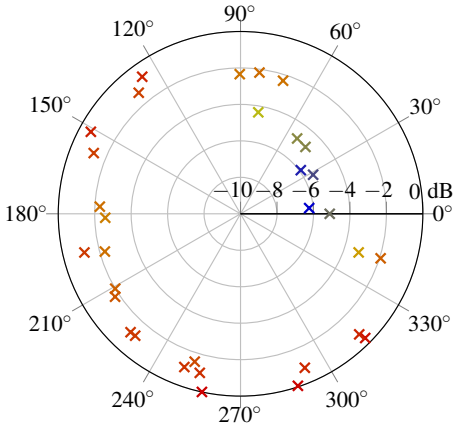

Fig. 4. Variation of the response of the element 6 with different phase states at 28 GHz. The amplitude is in dB and normalized to the maximum. Phase state 1 is considered as the reference phase shift, i.e. 0°.

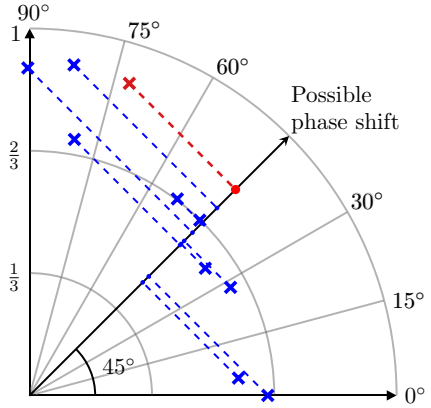

Fig. 5. Example how the projections of each phase state to the different phase shifts are evaluated. Phase shift in this example is $\theta = 45°$. The state highlighted in red gives the highest projected value and is chosen as a used phased state for this phase shift.

The results show that the states tend to be grouped together rather than being evenly distributed in the phase. Thus, no particular state can be found for phase shift angles from 90° to 120° nor for angles from 255° to 285°, leaving rather large arcs free in the unit circle. Furthermore, in the first 6 states, the arc from 0° to 60°, the output amplitudes are gravely (more than 4 dB) lower than the maximum amplitude achieved with state 25 at 255°. As rather similar behavior is seen with the other elements, it is obvious that the phase shifter states should be chosen according to the objective pattern shape and that it is a highly complex optimization task.

A. Gain Optimization Method

The main goal of the beam optimization is to achieve maximum gain towards the desired direction. From the single element perspective, the element should have the best possible amplitude and constructive element phasing to achieve this. The required phase shift is determined by the steering angle and is normalized to the chosen reference element.

First step in the gain optimization is to find out the best phase shifter state for the different phase shifts. This is done by making the projection of each phase state to the possible phase shifts. Phases from 0° to 359° with 1° steps are considered for the possible phase shifts, described as θ.

The linear phase state vectors that are normalized to the global measurement maximum are projected to the pointer indicating the required phase shift. The projected amplitude A_i of each phase state is calculated with

$$A_i(\theta) = a_i(\sin(\theta)\sin(\phi_i) + \cos(\theta)\cos(\phi_i)), \qquad (1)$$

where i indicates the phase state which is projected and i goes from 1 to 32. a_i is the normalized vector length and ϕ_i is the relative phase compared to State 1. The pointer is located at θ. The state giving the largest projection on that pointer is the one that is chosen to be used for that phase shift. An example showing how the correct state is chosen for the element 6 is presented in Fig. 5. The required phase shift in this example is $\theta = 45°$.

Thus, the best phase states and the corresponding projections are found for all the possible phase shifts for every array element forming a 16×360 matrix $\mathbf{P}$. The flow chart describing the optimization is presented in Fig. 6 with n indexing the element numbers from 1 to 16. Based on the beam steering, the progressive phase shifting is applied. Then the phase of the reference element (Element 1) is changed, which accordingly affects the required phase shift and the state in the other elements, resulting 360 possible phase state configuration options, indexed with j going from 1 to 360. This does not affect the direction of the beam itself as the relative phase shift between the elements remains the same. Following this, sums of the projected element amplitudes are calculated for each option. The one giving the highest total sum of the element amplitudes is chosen as the used configuration and the corresponding phase states are set for the antenna.

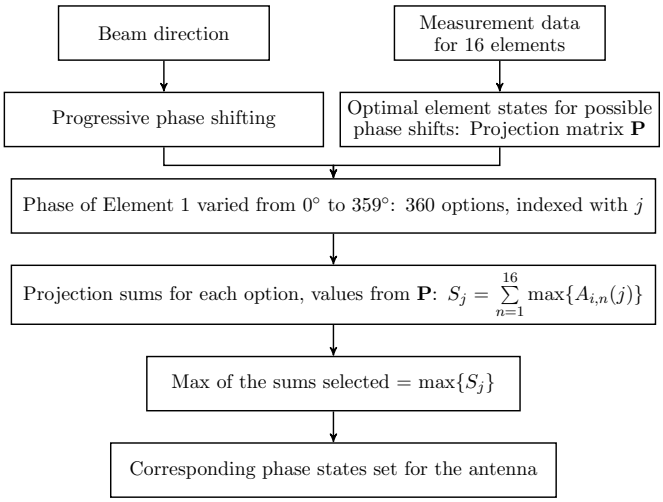

Fig. 6. Flow chart describing the gain optimization.

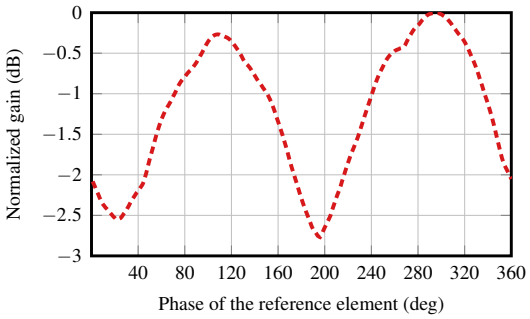

Fig. 7. Gain variation towards the broadside direction. Results are normalized to the plot maximum.

The total sum of the element amplitudes is directly related to the antenna gain towards the desired direction. The variation of the antenna gain due to the different phase shifter state configurations is shown in Fig. 7. Results are shown for the broadside beam in dB and they are normalized to the configuration providing the maximum gain.

The chosen configuration matters in the broadside quite much. This is explained by the feeding network configuration, which feeds the elements in the same array column with the same initial phase. This means that, e.g., the elements 1, 5, 9, and 13 have the same initial phase. However, at 28 GHz, the initial phase of the first and third column is relatively close to each other, only the third column phase is 360° delayed. Same phenomena is observed with the array columns 2 and 4. As a consequence, the elements in these columns have the phase shifter states that are very close to each other. The states have similar performance across all the elements, resulting in the broadside an effect where the states providing better amplitudes are visualized as plot maxima while the poorly working states are accordingly present as minima.

With the other steering angles this gain variation effect is not as strong. The effect is slightly present with azimuth steering, but not at all with the elevation steering, where the chosen states do scatter more randomly.

B. Taylor Optimization Method

The large variation in element amplitudes with different phase states inspires to optimize the beam in other ways as well. While the power division network does not allow other than uniform excitation, the element amplitudes can be controlled to some extent by choosing the proper phase states. Thus, an optimization goal is set to improve the side-lobe levels by choosing the element amplitudes according to an amplitude tapering scheme.

The amplitude weights are set to follow Taylor distribution. In the optimization algorithm, the goal is to find phase states that realize the required amplitudes while the phases can still realize the wanted beam steering. Thus, the allowed phase error for the elements is controlled in the algorithm to find the best element amplitudes that match the amplitude tapering, while providing the best gain. The beam patterns are then simulated based on the results and the ones with the lowest side lobes are chosen to be measured.

V. Measured Results

The optimization results are confirmed with the measurements. The phased array is measured with planar near-field scanner utilizing open-ended WR-28 waveguide as a near-field probe. The far-field patterns are acquired from the probe-corrected near-field results. Antenna gain is achieved by comparing the measured results to the one of the reference horn antenna.

A. Gain Optimization Results

The results of the gain optimized antenna characteristics with different steering angles at 28 GHz are collected to Table I. They are compared with the results from the non-optimized antenna.

TABLE I
Measured antenna characteristics before and after the gain optimization for different beam-steering angles at 28 GHz.

	Angle(°)	Realized Gain opti./orig. (dBi)	Side-lobe level opti./orig. (dB)
Broadside		12.0/10.6	−11.6/−10.0
Azimuth plane	10	11.5/10.7	−8.2/−15.5
	20	10.9/9.8	−7.1/−5.9
	30	9.5/7.5	−3.8/−2.9
	−10	11.8/10.8	−12.5/−7.9
	−20	10.8/9.8	−8.3/−6.2
	−30	9.8/9.3	−4.6/−4.3
Elevation plane	10	9.9/9.8	−6.1/−12.4
	20	6.7/6.6	−3.4/−6.2
	30	6.8/6.7	−0.9/−2.0
	−10	10.3/9.7	−10.8/−11.3
	−20	7.2/6.4	−1.8/−6.6
	−30	6.0/6.3	−0.6/−1.8

The gain optimization method works very well and the realized gain increases in almost all the steering angles towards the desired direction. Particularly the azimuth steering angles have better performance due to the optimization. Nevertheless, the side-lobe levels are not improving especially with the elevation angles. Furthermore, the rising grating lobes can be seen in the larger steering angles increasing the side-lobe level.

However, according to the simulations where the array factor and element factor are considered, the optimization method should give much better result than what is now achieved with elevation beam steering. Because the elements are measured independently while the others are turned off, the effect of the mutual coupling and the active impedance variation caused by it are not taken into account. It is assumed that the coupling is stronger in elevation (E-plane) and thus, the optimization is more affected in elevation beam steering. This is the only clear disadvantage of the optimization method, relying on individual element performance characterization. Still, the performance increase is quite remarkable.

To further highlight the effect of the gain optimization, the azimuth and elevation radiation pattern cuts of the broadside beam are presented in Fig. 8a and 8b, respectively. At broadside, the increase in the realized gain is 1.4 dB.

B. Taylor Optimization Results

Fig. 8 also shows the measurement results of the Taylor optimization at broadside. The Taylor optimized realized gain is 11.5 dBi while the side-lobe level is −12.4 dB, improving the gain by 0.9 dB and side-lobe level by 2.4 dB when compared to the original case without the optimization. In addition, Fig. 9 shows the measurement results of the radiation pattern comparison for the azimuth steering angles ±10° and ±20°. The results show how the Taylor optimization decreases the side lobes especially when compared to the maximum gain optimization, and also to the original situation.

Unfortunately, the effect in the elevation beam steering is not as good and no visible improvement due to the Taylor optimization can be seen. Again, this is thought to be due to the stronger coupling in the E-plane, which is present in the measurements but not in the optimization nor in the ideal simulations. However, the results in broadside and azimuth steering show that the Taylor optimization is clearly working and beneficial if the lower side lobes are required.

VI. Conclusion

The two beam optimization methods have been presented along with their measured results. The first method optimizes the realized gain towards the wanted steering angle, while the other method utilizes element amplitude variation to realize Taylor weighting in the array excitation. The gain maximization shows clear improvement in the antenna gain for both elevation and azimuth steering and the Taylor optimization improves the side-lobe level for the broadside and azimuth beams.

However, for both methods, the optimization in the elevation beam-steering does not produce as good results as with the azimuth beam-steering. This is assumed to be due to the stronger coupling in E-plane which changes the active impedance of the elements and, thus, the measured amplitudes and phases utilized in the optimization are not the same in the real case.

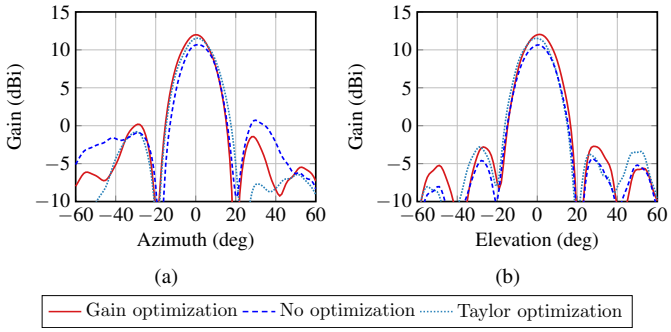

Fig. 8. Optimization results in broadside direction: (a) azimuth pattern, (b) elevation pattern.

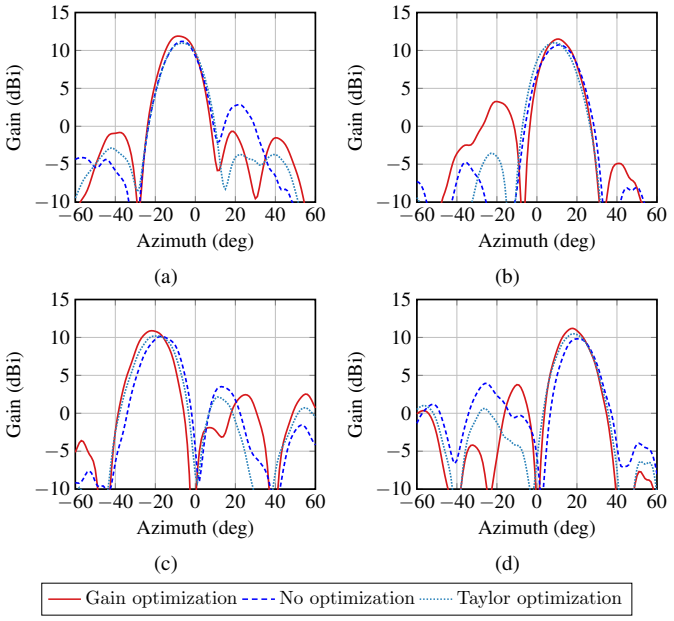

Fig. 9. Measured pattern comparison between gain optimization, no optimization, and Taylor optimization methods in azimuth directions: (a) −10°, (b) 10°, (c) −20°, and (d) 20° steering angle.

The presented optimization methods do not take into account the mutual coupling between the elements and this is clearest disadvantage of the utilized methods. Still the existing methods have proven to work fairly well for the purposes they have been designed for and are straightforward to apply.

Acknowledgment

The work of M. K. Leino was supported by the Walter Ahlström Foundation.

References

[1] R. J. Mailloux, *Phased Array Antenna Handbook*, 3rd ed. Norwood, MA, USA: Artech House, Inc., 2017.

[2] K. Carver, W. Cooper, and W. Stutzman, "Beam-pointing errors of planar-phased arrays," *IEEE Transactions on Antennas and Propagation*, vol. 21, no. 2, pp. 199–202, Mar. 1973.

[3] S. H. Son, W. Hwang, and S. I. Jeon, "Gain enhancement of large phased array antennas by phase error correction," in *2007 IEEE Antennas and Propagation Society International Symposium*, Jun. 2007, pp. 137–140.

[4] N. Nakamoto, T. Takahashi, Y. Konishi, and I. Chiba, "Phase optimization for accurate beam forming of phased array with element field errors at every phase shift," in *2013 IEEE International Symposium on Phased Array Systems and Technology*, Oct. 2013, pp. 693–697.

[5] M. Fakharzadeh, P. Mousavi, S. Safavi-Naeini, and S. H. Jamali, "The effects of imbalanced phase shifters loss on phased array gain," *IEEE Antennas and Wireless Propagation Letters*, vol. 7, pp. 192–196, 2008.

[6] T. Mitani, S. Tanaka, and Y. Ebihara, "Experimental study on one-dimensional phased array antenna including lossy digital phase shifters for transmitting power maximization," in *2011 XXXth URSI General Assembly and Scientific Symposium*, Aug. 2011, pp. 1–4.

[7] M. K. Leino, M. M. Islam, J. Ala-Laurinaho, and V. Viikari, "Diagnostics of the phased array for E-band using holography data," in *2018 48th European Microwave Conference (EuMC)*, Sep. 2018, pp. 1457–1460.

[8] M. K. Leino, R. Montoya Moreno, J. Ala-Laurinaho, R. Valkonen, and V. Viikari, "Waveguide-based phased array with integrated element-specific electronics for 28 GHz," *IEEE Access*, vol. 7, pp. 90 045–90 054, 2019.